# Thin Film PZT-Based PMUT Arrays for Deterministic Particle Manipulation

Christopher Y. Cheng, *Member, IEEE*, Ajay Dangi, *Member, IEEE*, Liqiang Ren, Sudhanshu Tiwari, Robert R. Benoit, *Member, IEEE*, Yongqiang Qiu, *Member, IEEE*, Holly S. Lay, *Member, IEEE*, Sumit Agrawal, Rudra Pratap, *Senior Member, IEEE*, Sri-Rajasekhar Kothapalli, Thomas E. Mallouk, Sandy Cochran, *Member, IEEE*, and Susan Trolier-McKinstry, *Fellow, IEEE*

***Abstract*— Lead zirconate titanate (PZT)-based piezoelectric micromachined ultrasonic transducers (PMUTs) for particle manipulation applications were designed, fabricated, characterized, and tested. The PMUTs had a diaphragm diameter of 60 $\mu$m, a resonant frequency of ∼8 MHz, and an operational bandwidth ($BW$) of 62.5%. Acoustic pressure output in water was 9.5 kPa at 7.5 mm distance from a PMUT element excited with a unipolar waveform at 5 $V_{pp}$. The element consisted of 20 diaphragms connected electrically in parallel. Particle trapping of 4 $\mu$m silica beads was shown to be possible with 5 $V_{pp}$ unipolar excitation. Trapping of multiple beads by a single element and deterministic control of particles via acoustophoresis without the assistance of microfluidic flow were demonstrated. It was found that the particles move toward diaphragm areas of highest pressure, in agreement with literature and simulations. Unique bead patterns were generated at different driving frequencies and were formed at frequencies up to 60 MHz, much higher than the operational BW. Levitation planes were generated above the 30 MHz driving frequency.**

***Index Terms*— Acoustic tweezing, arrays, microelectromechanical systems (MEMS), particle manipulation, piezoelectric micromachined ultrasonic transducers (PMUTs).**

Manuscript received March 7, 2019; accepted June 26, 2019. Date of publication July 2, 2019; date of current version September 25, 2019. This work was supported in part by the Center for Nanoscale Science, Materials Research Science and Engineering Center (MRSEC), and funded by the National Science Foundation under Grant DMR-1420620. C. Y. Cheng was supported by the National Defense Science and Engineering Graduate (NDSEG) Fellowship Program. A. Dangi was supported by the National Institute of Biomedical Imaging and Bioengineering (NIBIB), Center of National Institute of Health through the Post-Doctoral Fellowship awarded to Dr. Kothapalli under Grant R00EB017729-04. *(Corresponding author: Christopher Y. Cheng.)*

C. Y. Cheng and S. Trolier-McKinstry are with the Department of Materials Science and Engineering, Pennsylvania State University, University Park, PA 16802 USA, and also with the Materials Research Institute, Pennsylvania State University, University Park, PA 16802 USA (e-mail: cyc5@psu.edu; set1@psu.edu).

A. Dangi, S. Agrawal, and S.-R. Kothapalli are with the Department of Biomedical Engineering, Pennsylvania State University, University Park, PA 16802 USA (e-mail: axd571@psu.edu; sua347@psu.edu; szk416@psu.edu).

L. Ren is with the Department of Engineering Science and Mechanics, Pennsylvania State University, University Park, PA 16802 USA (e-mail: lzr144@psu.edu).

S. Tiwari and R. Pratap are with the Centre for Nano Science and Engineering, Indian Institute of Science, Bengaluru 560012, India (e-mail: sudhanshut@iisc.ac.in; pratap@iisc.ac.in).

R. R. Benoit is with the Sensors and Electron Devices Directorate, Army Research Laboratory, Adelphi, MD 20783 USA (e-mail: robert.r.benoit7.civ@mail.mil).

Y. Qiu is with the Department of Electronics and Electrical Engineering, Liverpool John Moores University, Liverpool L3 3AF, U.K. (e-mail: y.qiu@ljmu.ac.uk).

H. S. Lay is with FUJIFILM VisualSonics, Inc., Toronto, ON M4N 3N1, Canada (e-mail: holly.susan.lay@gmail.com).

T. E. Mallouk is with the Department of Chemistry, Pennsylvania State University, University Park, PA 16802 USA (e-mail: lzr144@psu.edu; tem5@psu.edu).

S. Cochran is with the James Watt School of Engineering, University of Glasgow, Glasgow G12 8QQ, U.K. (e-mail: sandy.cochran@glasgow.ac.uk).

This article has supplementary downloadable material available at http://ieeexplore.ieee.org, provided by the authors.

Digital Object Identifier 10.1109/TUFFC.2019.2926211

## I. Introduction

THERE is a growing interest in devices to independently and deterministically manipulate microscale objects, particularly in the biological sciences. Various contact and noncontact technologies have been developed to meet this demand. Noncontact methods are strongly preferred in biology as they maintain the integrity of cells and minimize interference with intercellular and intracellular processes [1], [2].

Of the reported noncontact methods, optical tweezers, dielectrophoresis, magnetophoresis, and acoustophoresis have been used for particle manipulation. Acoustophoresis is particularly attractive for biological applications as it does not require labeling, has no known toxic effects, and can maintain cell integrity during operation [3]–[6].

Many ultrasonic transducer designs have been explored for acoustic tweezing, as shown in Fig. 1. Unlike transducers for imaging, these are required only to transmit energy, and not to act additionally as receivers. Conventional transducers based on bulk piezoelectric materials or piezocomposites with front and back electrodes, Fig. 1(a), often have a matching layer to enhance energy transfer between the high acoustic impedance of the device and the low acoustic impedance of the medium. A backing layer may also be used to dampen ringing or reflect acoustic energy back to the front surface. However, conventional transducer structures constrain the geometry and hence operating frequencies and electrical impedance matching of the small elements in 2D arrays for particle manipulation applications.

In contrast, micromachined ultrasonic transducers (MUTs) prepared using microelectromechanical systems (MEMS)

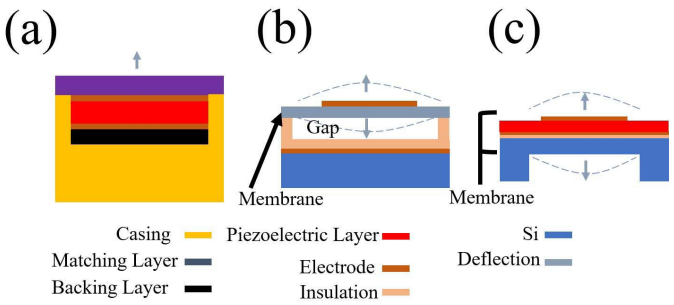


Fig. 1. Typical architectures of (a) bulk piezoelectric transducer, (b) CMUT, and (c) PMUT (after [7]).

fabrication techniques that allow ultrasonic arrays to be configured flexibly, with high spatial resolution, from many small diaphragms. They also offer intrinsically good acoustic matching and operating bandwidth (*BW*) and the potential for excellent electrical impedance matching. Two distinct platform technologies have emerged: capacitive MUTs (CMUTs) and piezoelectric MUTs (PMUTs).

CMUTs are based on flexural vibrations of a membrane caused by varying electrostatic attraction to a substrate. They can generate adequate acoustic pressures for medical imaging and particle trapping [8], [9]. They also integrate well with silicon electronics for voltage amplification and detection. However, they need high direct current (DC) bias voltages (30–100 V) to operate, often near the collapse voltage [10], [11], and this has led to an interest in devices that do not require biasing. PMUTs, which accomplish membrane deflection through lateral strain induced by the piezoelectric effect, meet this need. Generally, they have higher capacitances than CMUTs and thus lower electrical impedance, facilitating impedance matching to electrical circuitry. In addition, unlike in bulk piezoelectric transducers, the resonant frequency of a PMUT is not solely dependent on the thickness of the piezoelectric layer but is defined by a range of parameters including density, flexural rigidity, diaphragm radius, and shape of the membrane [7], [12]–[14]. Therefore, PMUTs offer significant freedom in their design.

Particle manipulation and trapping via acoustophoresis have been achieved in a variety of platforms, including transducers with interdigitated electrodes that use surface acoustic waves (SAWs) to trap particles in the pressure wave antinodes [6], [15], [16], transducers that use standing bulk acoustic waves in a channel for droplet sorting [17], and single beam acoustic transducers (SBATs) for particle and cell manipulation [18], [19]. These techniques have demonstrated high efficiency in particle sorting and trapping. SAW-based devices and SBAT often require higher voltage input or a power amplifier during operation ($>10$ $V_{\text{pp}}$ operation) [19], [20], and the manipulation is often confined to a few wavelengths away from the substrate. Similarly, SBAT requires higher voltage operations and is difficult to fabricate in arrays, and thus may not have the manipulation precision and design freedom of PMUTs. While particle trapping has recently been shown to be possible with CMUTs [8], [9], to date, it has not been extensively demonstrated with PMUTs. In addition, the important task of bulk manipulation of particles from element to element in an array has been demonstrated with MUTs only with heavy reliance on microfluidic flow, although there have been such demonstrations in bulk and thick film transducers [21]–[25]. Furthermore, particles have been reported to agglomerate toward the center of MUT diaphragms when the MUT is excited at the fundamental resonant frequency [8], [9]. While this fundamental mode thus enables particle trapping, the use of higher frequencies has not been extensively explored. If adequate pressures can be generated at higher modes, particles may be systematically manipulated in correspondence with the vibration mode of the diaphragm, allowing dynamic patterning with a single element.

In this paper, 1D PMUT arrays of multiple elements, each comprising many diaphragms connected electrically in parallel, are demonstrated through their manipulation of 4 $\mu$m $SiO_2$ particles via acoustophoresis without the assistance of microfluidic flow. It is also shown that bead patterns can be formed outside the operating *BW* of the devices, with the formation of bead patterns taking place over a wide frequency range.

## II. Design, Fabrication, and Experimental Setup

### A. Design

The resonant frequency (fundamental mode) of a PMUT, $f_{fr}$, with a circular clamped diaphragm is given by: [12]–[14]

$$f_{fr} = \alpha^2 / a^2 \sqrt{D_e / \sum_i \rho_i h_i} \tag{1}$$

where $\alpha$, $a$, $D_e$, $\rho_i$, and $h_i$ are the frequency parameter constant (equal to $\sim$3.196 for a clamped circular diaphragm), the radius of the PMUT, the flexural rigidity of the diaphragm, the density of the $i^{\text{th}}$ material in the stack forming the diaphragm, and the thickness of the $i^{\text{th}}$ material, respectively. Based on (1) and the material stack described in Section II-B, a diaphragm diameter of 60 $\mu$m was chosen to achieve a fundamental resonant frequency, $f_{\text{fr}} = 10$ MHz; 10 MHz was selected due to half the wavelength of the fundamental frequency in water, $\lambda_{\text{fr}}/2 \approx 75$ $\mu$m, is on the order of the dimensions of most cells, bacteria, and enzymes [26]–[28]. This increases the possibility of successful acoustophoretic manipulation. The diaphragms were separated by a 15 $\mu$m gap with a pitch of 75 $\mu$m, corresponding to $\lambda_{\text{fr}}/2$. The top electrode diameter was set to 65% of the diaphragm diameter to increase deflection [29]–[31].

### B. Fabrication

The full fabrication process for a PMUT is shown in Fig. 2. The base substrate was a silicon on insulator (SOI) wafer with a 2 $\mu$m Si thickness and a 2 $\mu$m buried thermal oxide layer (Ultrasil Corporation, Hayward, CA, USA). A $SiO_2$ passive elastic layer $\sim$0.16 $\mu$m thick was grown on both sides of the wafer by wet oxidation. Then 30 nm of Ti was sputtered on the device side, followed by rapid thermal annealing with 10 sccm of oxygen flow for 15 min at 700 °C to form $TiO_2$. This generates a well oriented 100-nm bottom electrode layer when Pt is sputtered at $>$500 °C [32].

To achieve the highly oriented {001} PZT films needed for optimal functional performance in applications, a thin

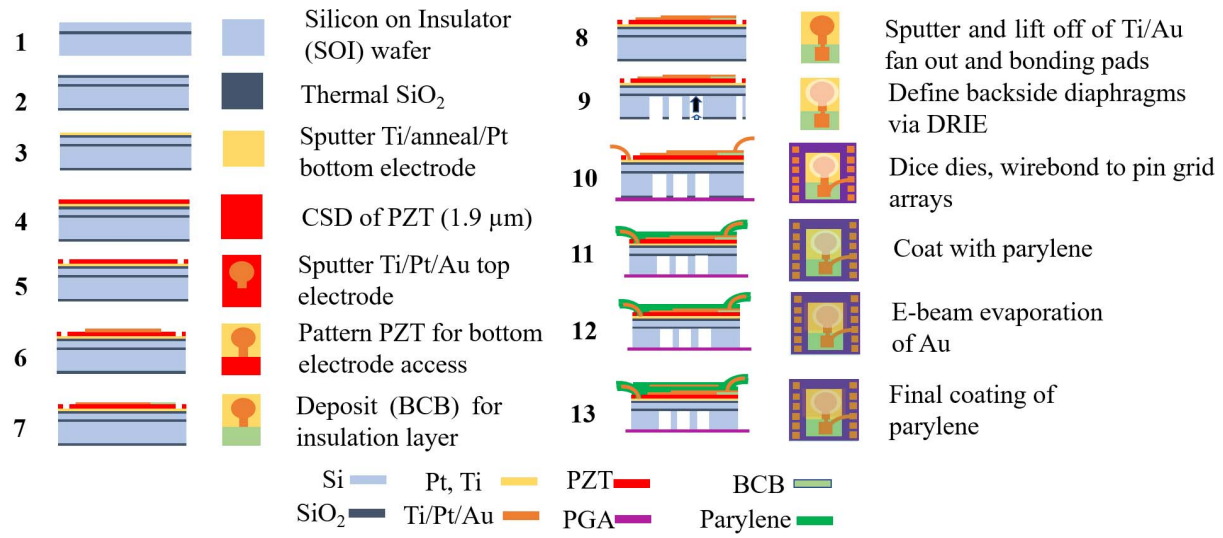


Fig. 2. PMUT fabrication process with cross-sectional and top-view of the fabricated PMUT.

$Pb(Zr_{0.52}Ti_{0.48})O_3$ sol–gel solution with 2% Nb and 20 mol.% excess Pb (Mitsubishi Materials Corporation, Sanda, Japan) was first spun on the wafer at 6000 rpm for 30 s as the seed layer [33], [34]. The seed layer was then pyrolyzed at 200 °C for 150 s before crystallization via rapid thermal annealing in a Pb-rich environment at 700 °C for 1 min. For the functional thin film PZT layer, 14 mol.% lead excess $Pb(Zr_{0.52}Ti_{0.48})O_3$ solution doped with 2% Nb (Mitsubishi Materials Corporation) was spun on at 2750 rpm for 45 s. The film was then pyrolyzed at 100 °C for 1 min and 300 °C for 4 min, followed by crystallization in a lead-rich rapid thermal annealer for 1 min at 700 °C. This process was repeated until a total thickness of 1.9 $\mu$m was achieved. Typically, 20 repeats were needed. Afterward, a thin PbO capping layer was deposited at 6000 rpm for 45 s with the same pyrolysis and crystallization steps as the PZT layers to remove pyrochlore from the surface of the film.

The top electrode was formed by sputtering 2 nm Ti as an adhesion layer followed by 50 nm of Pt without breaking the vacuum. The top electrode was annealed at 600 °C for 1 min before an additional 500 nm of Au was deposited and patterned to complete the top electrode. Access to the bottom electrode in areas not covered by the top electrode was gained by ion milling. An insulation layer was created by spinning and curing 0.9 $\mu$m thick bis(benzocyclobutene) to reduce parasitic capacitance over the areas defining the fan-out and bonding pads. These were subsequently patterned via liftoff and ~30 nm Ti and 500 nm Au were sputtered without breaking the vacuum. The devices were then released via silicon deep reactive ion etching (DRIE).

The wafer was diced into individual PMUT dies. These were mounted in the cavity of a pin grid array (PGA) (Spectrum Semiconductor Materials, San Jose, CA, USA) with silver paste to prevent water leakage from the backside. Electrical connections were made with wire bonding and coated conformally with ~4 $\mu$m of parylene for waterproofing. An equipotential plane was formed to eliminate dielectrophoresis in the particle manipulation experiments by depositing a 100 nm thin film of Au with e-beam evaporation. A second protective layer of parylene (~2 $\mu$m) was then coated onto the device. Prior to the characterization of the PMUT and the particle manipulation experiments, the array elements were poled at twice the coercive field of the PZT films for 15 min at room temperature.

### C. Experimental Setup

For particle manipulation experiments, two linear types of PMUT arrays were tested: a 1D array in which each element comprised one single diaphragm (referred to here as E1) and a 1-D array in which each element consisting of 20 diaphragms (referred to here as E20). In each case, the PGA cavity was filled with distilled water with varying concentrations of 4 $\mu$m $SiO_2$ beads (Sigma Aldrich, St. Louis, MO, USA). $SiO_2$ beads with 4 $\mu$m diameter were chosen as they were readily available. The water/air interface at the top of the cavity served as an acoustic reflector to generate standing waves. The PMUT elements were driven with continuous sinusoidal waves of amplitude 5 $V_{pp}$ and a 2.5 $V_{DC}$ offset unless otherwise stated.

## III. Simulations

It has been reported that acoustic tweezing with a single-beam CMUT source is based on gradient forces arising from the fluctuation of the generated pressure field when the source is activated. The gradient forces move particles to local/global acoustic pressure maxima or minima, depending on the properties of the particle [8], [9]. When a PMUT diaphragm is excited at resonance, the first mode results in the highest diaphragm deflection and highest pressure in the acoustic medium at the center, and the least deflection and pressure at the periphery of the diaphragm. Therefore, the maximum acoustic potential gradient arises between the center and edge of the diaphragm.

To describe how the particles should move in a pressure field, the acoustic potential can be related to the acoustic radiation force, $F_{\text{rad}}$, via Gor'kov's model

$$F_{\text{rad}} = -V * \left[ \frac{f_1}{2} \beta_m \nabla \langle p_s^2 \rangle - \frac{3 f_2}{4} \rho_m \nabla \langle v_s^2 \rangle \right] \tag{2}$$

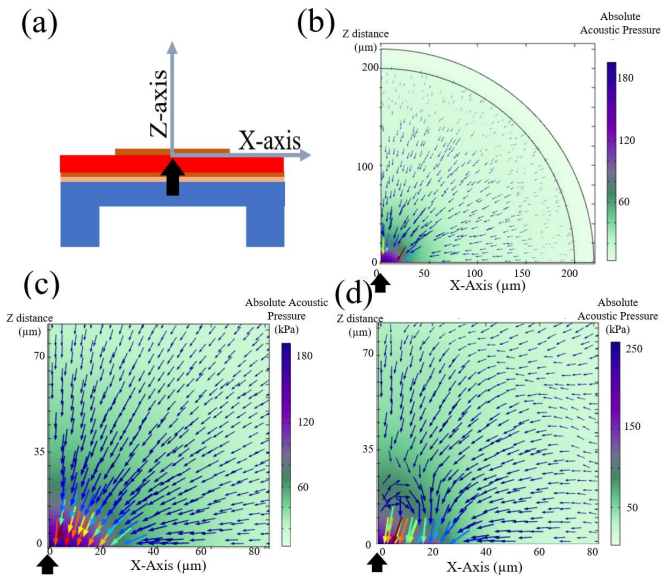


Fig. 3. Pressure fields generated by a single 60 $\mu$m diaphragm and particle movement for (b) and (c) fundamental mode and (d) second harmonic (0,2) mode. Arrows indicate the direction of $SiO_2$ beads particle movement. The colored arrows in (c) and (d) indicate the acoustophoretic force exerted on the particle. The length of the arrows corresponds to the relative force. The simulations were done for an axisymmetric model; only 1/2 of the diaphragm is shown with the center at the origin as indicated by the black arrows. A point of reference is shown in (a). Note the model used was a planar simulation with symmetry along the out-of-plane axis. This $X$–$Z$ view is also used for Fig. 4. A physically matched layer was used at a 200 $\mu$m distance from the membrane surface to prevent excitation of standing waves. An animation is presented in the Supplemental Materials.

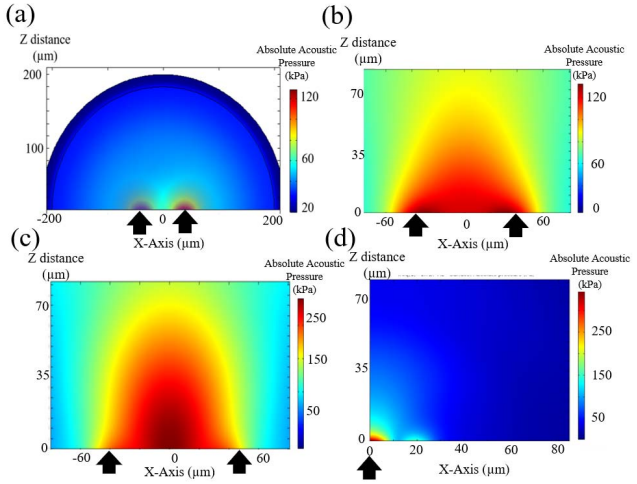


Fig. 4. (a) Individual pressure fields generated by two 60 $\mu$m diaphragms with 75-$\mu$m pitch, with each diaphragm excited individually and their individual pressure fields overlaid. (b) Pressure field generated by two diaphragms excited in unison at resonance. (c) Pressure field generated by two diaphragms excited in unison at 40% above the resonant frequency. (d) Pressure field generated by a single diaphragm excited at the second harmonic mode. Black arrows indicate the center of the diaphragms. The pressure fields overlapping in (a) and (b) indicate the potential for particles to move from one diaphragm to another. A physically matched layer was used at a 200 $\mu$m distance from the membrane surface to prevent excitation of standing waves.

where $V$ is the volume of the particle and the terms in the brackets relate to the acoustic potential, $\beta_m$ is the compressibility of the medium in which the particle is suspended, $\rho_m$ is the density of the medium, $v_s$ is the acoustic velocity, and $p_s$ is the pressure on the particle [8], [9], [35]–[37]. The terms $f_1$ and $f_2$ are coefficients given by

$$f_1 = 1 - \frac{\beta_s}{\beta_m} \tag{3}$$

$$f_2 = \frac{2(\rho_s - \rho_m)}{2\rho_s + \rho_m} \tag{4}$$

where $\beta_s$ and $\rho_s$ are the compressibility and density of the particle, respectively [8], [9], [36], [37]. Equations (2)–(4) were defined in COMSOL Multiphysics (COMSOL, Inc., Burlington, MA, USA) for a single PMUT diaphragm, with 4 $\mu$m $SiO_2$ beads as the particles to be manipulated.

The results in Fig. 3 show that when a diaphragm is excited, particles agglomerate at the center and close to the surface of the diaphragm, in areas of high acoustic pressure. Similar behavior is reported in the literature but with CMUTs as the ultrasound source [8], [9]. Fig. 4 shows the pressure fields generated by a pair of diaphragms, simulated with COMSOL. It can be seen that the pressure fields generated by individual diaphragms overlap with adjacent diaphragms. Also, the particle movement caused by one diaphragm in Fig. 3 draws particles as far as 200 $\mu$m from a diaphragm center. It was calculated from COMSOL that close to the PMUT surface, the acoustic force was approximately ~10 pN, and the effect of gravity force is two orders of magnitude lower (~0.4 pN). At approximately 50 $\mu$m away from the PMUT surface, the acoustic force is on the same order of magnitude as the gravity force. Thus, the particles were expected to move very close to the PMUT surface. In addition, if the pressure field is sufficiently large in extent and the distance between elements is sufficiently close, beads can potentially move from one element to another without assistance from the microfluidic flow. This possibility was deliberately increased by designing the PMUT elements with a pitch of 75 $\mu$m, corresponding to $\lambda_{fr}/2$ at 10 MHz in water.

In addition to those generated by the fundamental mode, patterns generated by different modes could potentially be useful. From the results shown in Figs. 3 and 4, different vibrational modes should generate different bead patterns based on the resultant pressure field. For example, the (0, 2) mode would occur at a frequency approximately 3.89 times the fundamental (0, 1) mode frequency of a clamped circular plate [38]. For the (0, 2) mode, the pressure field is shown in Figs. 3(d) and 4(d). This suggests there would be two areas where the beads could agglomerate: at the center of the diaphragm and in a circular node around the center of the diaphragm.

Figs. 3 and 4 were produced with a physically matched layer positioned at 200 $\mu$m vertically from the membrane surface to prevent excitation of standing waves. If this is removed, allowing reflection, and the distance between the PMUT and the reflecting surface is multiple half-wavelengths, large pressure fields can be generated and correspondingly higher acoustic field amplitudes that can cause particles to move to levitation planes (LPs) at the acoustical nodes [39]. The positions of the LPs normal to the acoustic source direction can be expressed as

$$\text{LP} = n \cdot \lambda/4 \tag{5}$$

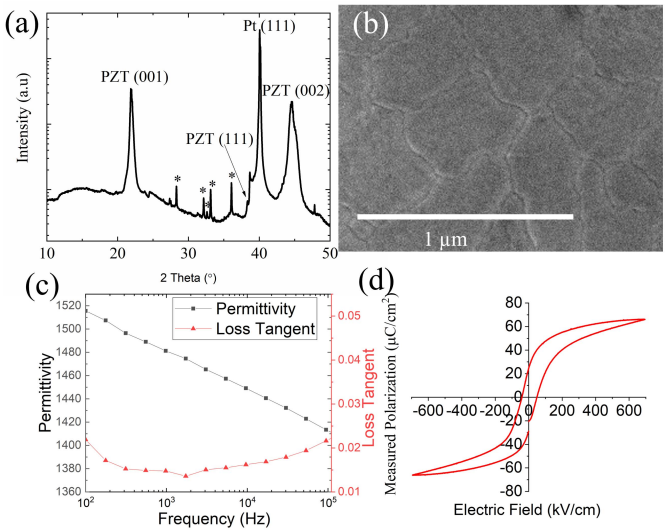


Fig. 5. Results of structural analysis of PZT via (a) XRD and (b) FESEM. Phase-pure perovskite was achieved with chemical solution deposition. No visible pyrochlore or secondary phases were found. Asterisks (∗): substrate peaks. Measurements of (c) dielectric permittivity, loss tangent and (d) hysteresis loops indicate permittivity >1400, loss tangent <3%, remanent polarization ∼24 $\mu$C/cm$^2$, and coercive field ∼50 kV/cm.

where $n$ and $\lambda$ are a whole integer and the acoustic wavelength, respectively. The depth of the water in the PGA cavity was not controlled systematically in this study; however, LPs can be more readily formed if the cavity height is a multiple of the driving wavelength. Such planes increase in number if the driving frequency is high, as the number of nodal planes in a fixed distance increases with driving frequency.

## IV. PMUT Characterization

For a high-quality PMUT, the PZT quality needs to be high. X-ray diffraction (XRD) and field-emission scanning electron microscopy (FESEM) were used to confirm that the PZT films were phase-pure perovskites and highly {001} oriented as shown in Fig. 5. The relative permittivity, $\varepsilon_r$, and loss tangent, tan $\delta$, were measured for 20 different elements in an array to test for the uniformity after the entire process was completed. Hysteresis loops were also measured to confirm the quality of the PZT. The electrical measurements are also presented in Fig. 5. At 95% confidence interval at 1 kHz, $\varepsilon_r = 1487 \pm 8$ and tan $\delta = 1.40 \pm 0.06\%$, respectively, indicating high uniformity between elements. The remanent polarization, $P_r$, was ≈24 $\mu$C/cm$^2$, and the coercive field, $E_C$, was ≈50 kV/cm.

Laser Doppler vibrometry (LDV) was used to evaluate $f_{fr}$ and the field-induced deflection of the fabricated device. The results are shown in Fig. 6. It was found that, for PMUTs on the same wafer, $6 < f_{fr} < 8$ MHz, due primarily to the footing effect in the DRIE process which changes the diaphragm diameter. Within a given die, the values of $f_{fr}$ were well-matched with larger variations observed across the 4″ wafer. Higher modes can also be seen at 13.0 and 19.8 MHz, which correspond to the (1, 1) and (0, 2) modes, respectively [38]. The LDV instrument (Polytec GmbH, Walbronn, Germany) could record a maximum deflection signal of only 79 nm, hence, for higher driving voltages, the center deflections seen

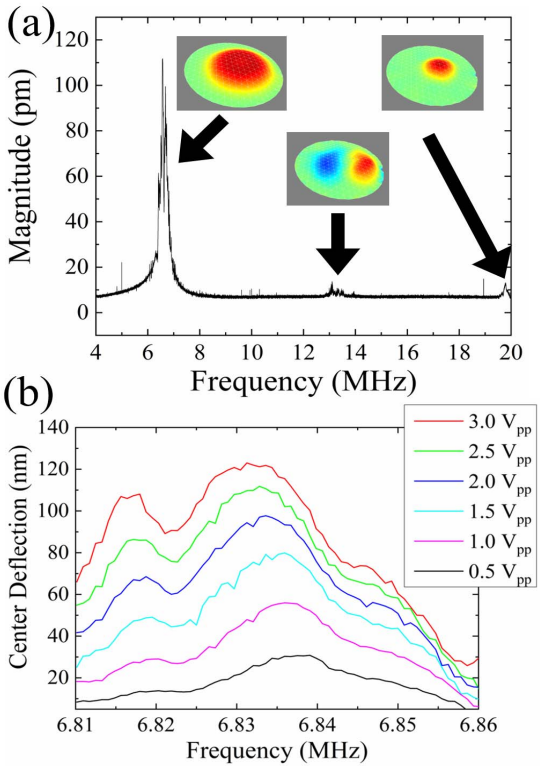


Fig. 6. LDV measurements in the air showing center deflection spectra (a) over a wide frequency range at 0.5–3.0-$V_{pp}$ driving voltage via laser chirp measurement and (b) close to resonance via peak hold measurement. Higher frequency modes are seen in (a) at 13 and 19.5 MHz. The measurements here were from the same batch of devices used in later experiments.

in Fig. 6(b) were extrapolated from the deflections near the diaphragm periphery, where motion is more strongly clamped. Using this technique, the deflection profiles indicate that in air, high deflections (∼40 nm/V) can be achieved for low driving voltages for both the E1 and E20 arrays.

The pressure output, $P$, and $BW$ were evaluated for the E20 array. The array was placed in an acrylic water tank and operated in a transmit mode while a hydrophone (HGL-0085, Onda, Inc., Sunnyvale, CA, USA) acted as a receiver at 7.5 mm distance from the surface of the transducer. One element was excited with a 5 $V_{pp}$ unipolar sinusoidal burst of five cycles to measure $P$. For $BW$, the same unipolar voltage excitation was used but with a single-cycle sinusoid at the resonant frequency, and a total of 59 dB gain was used to amplify the signal. A Fourier transform was then used to calculate BW at −6 dB. The results are shown in Fig. 7. An element of 20 diaphragms (E20) yielded an output pressure of ∼9.5 kPa at 7.5 mm and the BW at −6 dB was approximately 62.5%. The underwater resonance frequency was found to be ∼8 MHz.

## V. Particle Manipulation

For particle manipulation experiments, the PMUT elements were excited below $f_{fr}$ with a unipolar signal at 5 $V_{pp}$ with a function generator and with a low concentration of 4 $\mu$m $SiO_2$ beads in the water medium. Results are shown in Fig. 8. The lower frequency was used because when an element is excited very close to the resonant frequency, as presented in Fig. 8(a) and (b), cross-coupling excited neighboring

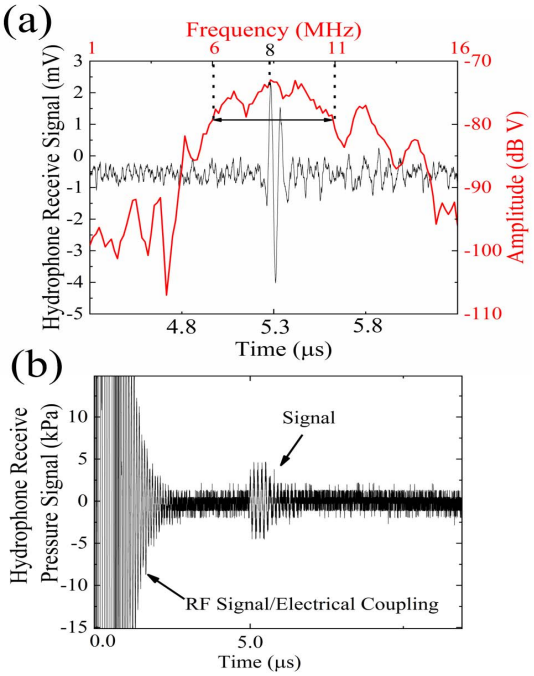


Fig. 7. Acoustic characterization of E20 array. (a) Time and frequency characteristics with single-cycle sinusoidal excitation (with 59 dB total gain) and (b) hydrophone output at $f_{fr}$ with five cycles sinusoidal excitation. The response was ~0.46 $\mu$V which corresponds to ~9.5 kPa at 5 $V_{pp}$ unipolar excitation at 7.5 mm distance from the PMUT. The BW at −6 dB was ~62.5% from the Fourier transformation of the signal response, with a center frequency of 8 MHz.

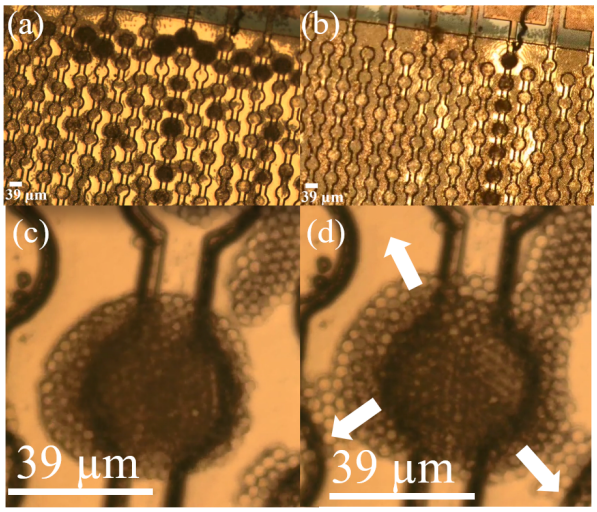


Fig. 8. $SiO_2$ bead patterns generated when the E20 array was excited at (a) ~6 MHz and (b) ~4.9 MHz. Cross-coupling is less severe below resonance, indicated by the much heavier clustering of particles at the excited element. Generally, the beads agglomerated most effectively with $f$ in the range 5–6 MHz. Higher density particle clustering was observed for (c) 5 $V_{pp}$ excitation than for (d) 1 $V_{pp}$ excitation; higher voltages caused tighter conglomeration of the beads than lower voltages. The white arrows indicate the direction that as the voltage is decreased, the bead cluster relaxed, and the diameter of the cluster decreased from (c) to (d) from ~60 to ~54 $\mu$m, respectively.

elements. At driving frequencies ($f$) ~18% below $f_{fr}$, the cross-coupling was much less severe.

It was observed that the bead clusters became more tightly packed, as seen in Fig. 8(c) and (d), as the applied unipolar voltage increased from 1 to 5 $V_{pp}$ with $f \approx f_{fr}$.

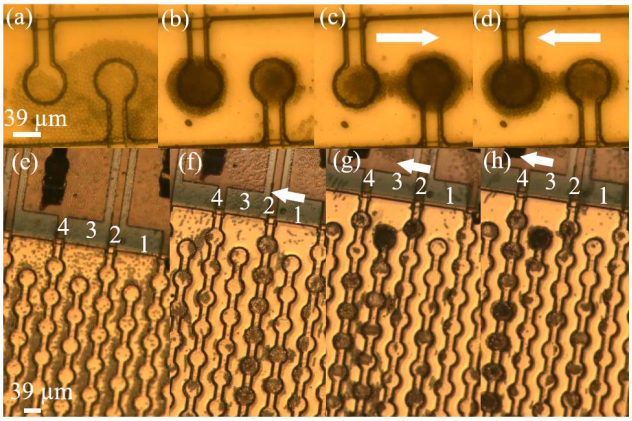


Fig. 9. Manipulation of 4-$\mu$m silica beads using two elements from (a)–(d) E1 and (e)–(h) E20 PMUT designs. The images show the $SiO_2$ beads when (a) elements are off, (b) both elements are turned on, (c) when the left element is switched off and the right element remains on, and (d) when the right element is switched off and the left element is switched on. Beads move from the element that is turned off to the element that is turned on. This technique was used when manipulating the beads with the E20 design, where beads were trapped and moved from element 1 to element 4. White arrow: direction of particle movement. Note the scale bars are consistent between (a)–(d) and (e)–(h).

Furthermore, the velocity of the beads toward the axis of the diaphragm increased as the excitation voltage increased and when $f_{fr}$ was approached. This is reasonable [8], [9] as higher deflections result in larger pressure outputs, generating larger pressure gradients and thus larger acoustic forces. The phenomenon of bead agglomeration toward the center of the diaphragm as the driving frequency approaches the resonant frequency corresponds to what has been reported for CMUTs [8], [9]. PMUTs not released by backside etching yielded no movement of the particles, showing that the particle manipulation arises from acoustophoresis.

In order to test control of particle motion in 1D, individual and adjacent elements of the E1 PMUT array were excited and nonexcited to facilitate particles moving to the generated local acoustic potential minimum. A similar excitation pattern was used on the E20 PMUT array to investigate whether particle trapping is possible over multiple diaphragms simultaneously when one array element was excited. The results are presented in Fig. 9.

When an element is turned on, nearby beads cluster over the center of the diaphragm and, when the element is turned off, the bead cluster disperses and moves toward neighboring elements that remain activated, due to the gradient in acoustic pressure, in agreement with the simulations presented in Figs. 3 and 4. This behavior was observed for both the E1 and E20 arrays. Because the pressure gradient increases between the center of a diaphragm and its periphery as $f$ approaches $f_{fr}$ [8], [9], the beads can be moved from one element to another by tuning the driving frequency. The relationship between frequency and wavelength and particle movement is complex; changing frequency results in changing deflection, which changes the output pressure as well as potential crosstalk, further complicating the acoustic potential gradient. In addition, changing frequency also changes wavelength, and thus also changes the acoustic potential gradient.

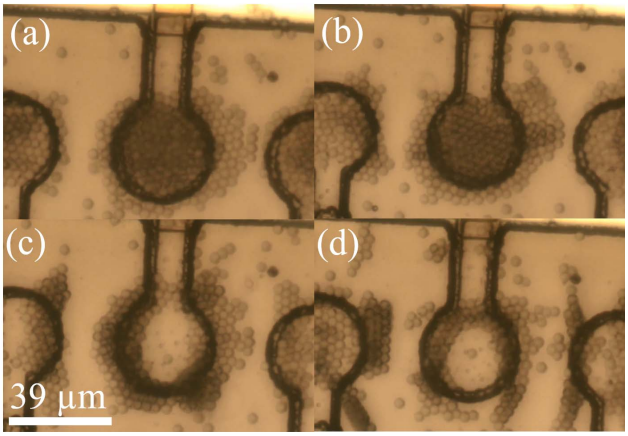


Fig. 10. Particle behavior stimulated by driving one element at frequencies (a) 5 MHz, (b) 13 MHz, (c) 17 MHz, and (d) 23 MHz. The scale bar applies to all of (a)–(d).

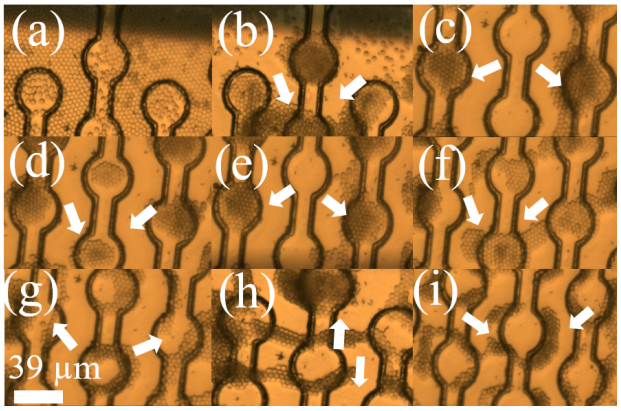


Fig. 11. Silica bead patterns generated using E20 with driving frequencies at (a) 1 MHz, (b) 3–6 MHz, (c) 7 MHz, (d) 8 MHz, (e) 9 MHz, (f) 13 MHz, (g) 17 MHz, (h) 18 MHz, and (i) 22 MHz. Arrow: directions of particle motion before the particles settle into their observed position. The scale bar applies to (a)–(i).

However, based on Fig. 4(c), when two diaphragms are excited above the resonant frequency, the area of highest pressure is between two diaphragms rather than directly over the diaphragms. By exciting the transducers at a frequency above resonance, the beads move to the highest areas of pressure and thus move to the areas between the two diaphragms. Then, the driving frequency can be changed to the resonant frequency, and thus the beads move to areas over the diaphragm more easily due to closer proximity to the generated highest-pressure zone, as was observed in the experiments.

The effects of different excitation frequencies on bead patterns and behavior over diaphragms in the E1 and E20 arrays are illustrated in Figs. 10 and 11, respectively. For the E1 array, again the beads agglomerate at the center of the diaphragm at $f_{fr}$. The beads remain at the center of the diaphragm until $f \approx 17$ MHz, where they begin to form an annulus. As $f$ approaches 23 MHz, two beads move toward the center of the diaphragm, while most stay in the nodal torus formed previously. The pattern in which the torus appears matches the simulated pressure field generated by the (0,2) mode shown in Fig. 4(d). If the resonant frequency is taken to be ~6 MHz (at which frequency the beads tended to agglomerate most effectively), 23 MHz is approximately 3.9 times $f_{fr}$, again matching theory [38]. The (1,1) mode was not seen via bead excitation. The in-plane stress in the piezoelectric layer induced by the electric field produces a uniform bending moment along the periphery of the top electrode. This favors radial modes instead of nonradial modes; hence, the amplitude of the (1,1) mode may be too low to cause acoustophoretic motion of beads [14], [38].

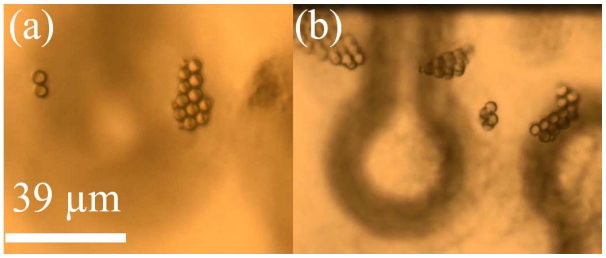


Fig. 12. LP of 4 $\mu$m $SiO_2$ beads when PMUTs E1 were excited at (a) 30 MHz and (b) 50 MHz. The LPs are identified in Table I. The LPs are evident due to the need to defocus the microscope from the PMUT surface and focus on areas above it. The scale bar applies to (a) and (b).

TABLE I
LP HEIGHTS AT DIFFERENT EXCITATION FREQUENCIES

| Driving Frequency (MHz) | Half wavelength value (μm) | Observed Levitation Plane Heights (from PMUT surface, μm) |
|---|---|---|
| 30 | 25 | 56, 74 |
| 50 | 15 | 19, 38, 51 |
| 60 | 12.5 | 10, 20 |

For the E20 device, similar patterns emerged; beads agglomerated at the center of each diaphragm when resonance was approached, and torus shapes were seen at approximately $f \approx 3.9 f_{fr}$. However, several unique behaviors were seen in elements with 20 diaphragms compared to elements with only 1 diaphragm, as shown in Fig. 11. Beads moved away from the excited diaphragm at 7 MHz and returned at 8 MHz. This behavior was also seen when transitioning from 9 to 13 MHz. One possible explanation can be drawn from the simulation illustrated in Fig. 4(c), where above $f_{fr}$, an acoustic potential well can encourage beads to move away from the diaphragm. When the elements are excited together, depending on the separation distance between elements and the excitation frequency, larger acoustic pressures may be generated between diaphragms, with the resulting gradient pushing the beads toward the higher pressure regions. Crosstalk from neighboring, nonelectrically excited elements may thus be the cause of behaviors as shown in Fig. 11(c)–(h).

At higher driving frequencies, even without precise control over the height of the chamber, LPs were also observed, as shown in Fig. 12, with the heights of the LPs indicated in Table I.

In some cases, multiple LPs were observed. The LPs form at heights that correspond approximately with $n\lambda/4$ as predicted by Equation (5). While the beads are trapped in the LP, they have little motion in the $X$ and $Y$ directions. It is noteworthy that these effects were observed far beyond the limits of the measured $BW$ of 62.5%.

## VI. Conclusion

PMUT arrays were successfully fabricated with high quality {001} oriented PZT that produced ∼9.5 kPa at 7.5 mm distance and 40 nm/V deflection in the air at 6–8-MHz resonant frequency. The arrays were shown to have the ability to control the location of $SiO_2$ beads and bead agglomerations in 1D (laterally) by selecting which PMUTs were excited. At higher excitation frequencies, different bead patterns were observed, with the potential for use for patterning cells and particles in ways other than the agglomeration at the diaphragm center demonstrated previously with CMUTs [8], [9]. Even well above the −6 dB BW of the fundamental resonant mode, LPs and bead patterning were observed, demonstrating generation of sufficient pressure to realize these effects at frequencies as high as 60 MHz.

This work opens a pathway toward 2D manipulation of particles via PMUT arrays. Of particular interest would be to assess whether asymmetric nanorods, cells, and proteins/enzymes can be manipulated with PMUTs. While preliminary data shows that biological cells move upon activation of the PMUT, it was difficult to deterministically manipulate the cells from element to element. This was attributed to the acoustic impedance mismatch between the medium (distilled water) and cells being much lower compared to distilled water and silica beads. Thus, it is difficult to manipulate with the current pressure outputs. In the future, this can be circumvented by either increasing the drive voltages, improving PMUT pressure output, or by manipulating bubbles in conjunction with the cells, as has been demonstrated in the literature [40]. In addition, PMUTs integrated into imaging systems will also be explored in the future.

## Appendix

Videos of particle manipulation are available online.

## Acknowledgment

The authors would like to thank Dr. C. Démoré at Sunnybrook Research Institute, Toronto, ON, Canada, for technical discussions.

## References

[1] J. Hultström, O. Manneberg, K. Dopf, H. M. Hertz, H. Brismar, and M. Wiklund, "Proliferation and viability of adherent cells manipulated by standing-wave ultrasound in a microfluidic chip," *Ultrasound Med. Biol.*, vol. 33, no. 1, pp. 145–151, Jan. 2007.

[2] D. Carugo *et al.*, "Contrast agent-free sonoporation: The use of an ultrasonic standing wave microfluidic system for the delivery of pharmaceutical agents," *Biomicrofluidics*, vol. 5, no. 4, Nov. 2011, Art. no. 044108.

[3] M. C. Ziskin and D. B. Petitti, "Epidemiology of human exposure to ultrasound: A critical review," *Ultrasound Med. Biol.*, vol. 14, no. 2, pp. 91–96, 1988.

[4] M. Wiklund, "Acoustofluidics 12: Biocompatibility and cell viability in microfluidic acoustic resonators," *Lab Chip*, vol. 11, no. 1, pp. 2018–2028, 2012.

[5] M. Evander *et al.*, "Noninvasive acoustic cell trapping in a microfluidic perfusion system for online bioassays," *Anal. Chem.*, vol. 79, no. 7, pp. 2984–2991, Feb. 2007.

[6] F. Guo, "Three-dimensional manipulation of single cells using surface acoustic waves," *Proc. Nat. Acad. Sci. USA*, vol. 113, no. 6, pp. 1522–1527, Feb. 2016.

[7] Y. Qiu *et al.*, "Piezoelectric micromachined ultrasound transducer (PMUT) arrays for integrated sensing, actuation and imaging," *Sensors*, vol. 15, no. 4, pp. 8020–8041, Apr. 2015.

[8] C. Samarasekera, J. G. W. Sun, Z. Zheng, and J. T. W. Yeow, "Trapping, separating, and palpating microbead clusters in droplets and flows using capacitive micromachined ultrasonic transducers (CMUTs)," *Sens. Actuators B, Chem.*, vol. 276, pp. 481–488 Dec. 2018.

[9] S. P. Mao *et al.*, "Capacitive micromachined ultrasonic transducers for acoustic manipulation," in *Proc. 18th Int. Conf. Solid-State Sensors, Actuat. Microsyst. (Transducers)*, Anchorage, AK, USA, Jun. 2015, pp. 662–665.

[10] A. S. Ergun, G. G. Yaralioglu, and B. T. Khuri-Yakub, "Capacitive micromachined ultrasonic transducers: Theory and technology," *J. Aerosp. Eng.*, vol. 16, no. 2, pp. 76–84. Nov. 2002.

[11] A. Nikoozadeh, B. Bayram, G. G. Yaralioglu, and B. T. Khuri-Yakub, "Analytical calculation of collapse voltage of CMUT membrane [capacitive micromachined ultrasonic transducers]," in *Proc. IEEE Ultrason. Symp.*, Montreal, QC, Canada, Aug. 2004, pp. 256–259.

[12] F. Sammoura, K. Smyth, S. Bathurst, and S.-G. Kim, "An analytical analysis of the sensitivity of circular piezoelectric micromachined ultrasonic transducers to residual stress," in *Proc. IEEE Int. Ultrason. Symp.*, Dresden, Germany, Oct. 2012, pp. 580–583.

[13] A. Dangi and R. Pratap, "System level modeling and design maps of PMUTs with residual stresses," *Sens. Actuators A, Phys.*, vol. 262, pp. 18–28, Aug. 2017.

[14] S. Timoshenko and S. Woinowsky-Krieger, *Theory of Plates and Shells*. Singapore: McGraw-Hill, 1959, pp. 1–568.

[15] L. Ren *et al.*, "Standing surface acoustic wave (SSAW)-based fluorescence-activated cell sorter," *Small*, vol. 14, no. 40, Oct. 2018, Art. no. 1801996.

[16] M. Wu *et al.*, "High-throughput cell focusing and separation via acoustofluidic tweezers," *Lab Chip*, vol. 18, pp. 3003–3010, Aug. 2018.

[17] I. Leibacher, P. Reichert, and J. Dual, "Microfluidic droplet handling by bulk acoustic wave (BAW) acoustophoresis," *Lab Chip*, vol. 15, no. 13, pp. 2896–2905, Jun. 2015.

[18] K. H. Lam, Y. Li, Y. Li, H. G. Lim, Q. Zhou, and K. K. Shung, "Multifunctional single beam acoustic tweezer for non-invasive cell/organism manipulation and tissue imaging," *Sci. Rep.*, vol. 6, Nov. 2016, Art. no. 37554.

[19] B. Zhu *et al.*, "Micro-particle manipulation by single beam acoustic tweezers based on hydrothermal PZT thick film," *AIP Adv.*, vol. 6, no. 3, Mar. 2016, Art. no. 35102.

[20] S. Li *et al.*, "Standing surface acoustic wave (SSAW)-based cell washing," *Lab Chip*, vol. 15, no. 1, pp. 331–338, Jan. 2015.

[21] A. Marzo and B. W. Drinkwater, "Holographic acoustic tweezers," *Proc. Nat. Acad. Sci. USA*, vol. 116, no. 1, pp. 84–89 Dec. 2018.

[22] S. Deng, K. Jia, E. Wu, X. Hu, Z. Fan, and K. Yang, "Controllable micro-particle rotation and transportation using sound field synthesis technique," *Appl. Sci.*, vol. 8, no. 1, p. 73, Jan. 2018.

[23] Y. Qiu *et al.*, "Screen-printed ultrasonic 2-D matrix array transducers for microparticle manipulation," *Ultrasonics*, vol. 62, pp. 136–146, Sep. 2015.

[24] C. Yoon, B. J. Kang, C. Lee, H. H. Kim, and K. K. Shung, "Multiparticle trapping and manipulation by a high-frequency array transducer," *Appl. Phys. Lett.*, vol. 105, no. 21, Nov. 2014, Art. no. 214103.

[25] H. Wang, Y. Qiu, C. Démoré, S. Gebhardt, and S. Cochran, "2-D crossed-electrode transducer arrays for ultrasonic particle manipulation," in *Proc. IEEE Int. Ultrason. Symp.*, Tours, France, Sep. 2016, pp. 1–4.

[26] N. Nama, R. Barnkob, Z. Mao, C. Kähler, F. Costanzo, and T. J. Huang, "Numerical study of acoustophoretic motion of particles in a PDMS microchannel driven by surface acoustic waves," *Lab Chip*, vol. 15, no. 12, pp. 2700–2709, May 2015.

[27] M. Antfolk, P. B. Müller, P. Augustsson, H. Bruus, and T. Laurell, "Focusing of sub-micrometer particles and bacteria enabled by two-dimensional acoustophoresis," *Lab Chip*, vol. 14, no. 15, pp. 2791–2799, May 2014.

[28] Y. Liu and K.-M. Lim, "Particle separation in microfluidics using a switching ultrasonic field," *Lab Chip*, vol. 11, no. 18, pp. 3167–3173, Aug. 2011.

[29] P. Muralt and J. Baborowski, "Micromachined ultrasonic transducers and acoustic sensors based on piezoelectric thin films," *J. Electroceram.*, vol. 12, nos. 1–2, pp. 101–108, 2004.

[30] R. Przybyla, "Ultrasonic 3D rangefinder on a chip," Ph.D. dissertation, Dept. Elect. Eng., Univ. California, Berkeley, CA, USA, 2013.

[31] Y. Lu and D. A. Horsley, "Modeling, fabrication, and characterization of piezoelectric micromachined ultrasonic transducer arrays based on cavity SOI wafers," *J. Microelectromech. Syst.*, vol. 24, no. 4, pp. 1142–1149, 2015.

[32] A. J. Fox, B. Drawl, G. R. Fox, B. J. Gibbons, and S. Trolier-McKinstry, "Control of crystallographic texture and surface morphology of Pt/$TiO_2$ templates for enhanced PZT thin film texture," *IEEE Trans. Ultrason., Ferroelectr., Freq. Control*, vol. 62, no. 1, pp. 56–61, Jan. 2015.
[33] T. M. Borman, S. W. Ko, P. Mardilovich, and S. E. Trolier-McKinstry, "Development of crystallographic texture in chemical solution deposited lead zirconate titanate seed layers," *J. Amer. Ceram. Soc.*, vol. 100, no. 10, pp. 4476–4482, Oct. 2017.
[34] T. M. Borman, W. Zhu, K. Wang, S. W. Ko, P. Mardilovich, and S. E. Trolier-McKinstry, "Effect of lead content on the performance of niobium-doped 100 textured lead zirconate titanate films," *J. Amer. Ceram. Soc.*, vol. 100, no. 8, pp. 3558–3567, Aug. 2017.
[35] L. Gor'kov, "On the forces acting on a small particle in an acoustical field in an ideal fluid," *Sov. Phys. Doklady*, vol. 6, p. 773. Mar. 1962.
[36] S. V. V. N. Kothapalli, M. Wiklund, B. Janerot-Sjoberg, G. Paradossi, and D. Grishenkov, "Investigation of polymer-shelled microbubble motions in acoustophoresis," *Ultrasonics*, vol. 70, pp. 275–283, Aug. 2016.
[37] H. Bruus, "Acoustofluidics 7: The acoustic radiation force on small particles," *Lab Chip*, vol. 12, no. 6, pp. 1014–1021, 2012.
[38] A. W. Leissa, *Vibration of Plates*. Washington, DC, USA: GPO, 1969, pp. 1–345.
[39] S. Zhao and J. Wallaschek, "A standing wave acoustic levitation system for large planar objects," *Arch. Appl. Mech.*, vol. 81, no. 2, pp. 123–139, Feb. 2011.
[40] A. van Wamel, A. Bouakaz, M. Versluis, and N. de Jong, "Micromanipulation of endothelial cells: Ultrasound-microbubble-cell interaction," *Ultrasound Med. Biol.*, vol. 30, no. 9, pp. 1255–1258, Sep. 2004.

**Christopher Y. Cheng** (M'17) received the B.S. degree (*cum laude)* in materials science and engineering and the B.S. degree (*cum laude)* in chemistry from the University of Minnesota at Twin Cities, Minneapolis, MN, USA, in 2016. He is currently pursuing the Ph.D. degree in materials science and engineering with Pennsylvania State University, University Park, PA, USA, with a focus on piezoelectric micromachined ultrasound transducers (PMUTs) and their applications.

He was an Intern at 3M Company, Maplewood, MN, USA, and the U.S. Army Research Laboratory, Adelphi, MD, USA. He is a National Science Foundation Graduate Research Fellow Awardee and a National Defense Science and Engineering Graduate Fellow.

**Ajay Dangi** (M'18) received the B.Tech. degree in mechanical engineering from IIT Varanasi, Varanasi, India, in 2010, and the Ph.D. degree in mechanical engineering from the Indian Institute of Science, Bengaluru, India, in 2016.

From 2016 to 2017, he was a Research Assistant with the MEMS Laboratory, Center for Nano Science and Engineering, Indian Institute of Science. Since 2017, he has been a Postdoctoral Scholar with the Department of Biomedical Engineering, Pennsylvania State University, University Park, PA, USA. His research interests include photoacoustic and ultrasound imaging, microelectromechanical system (MEMS)/Micro-Opto-Electro-Mechanical Systems sensors, piezoelectric micromachined ultrasound transducers (PMUTs), and acoustics.

**Liqiang Ren** received the B.S. degree in optics from the Harbin Institute of Technology, Harbin, China, 2010, the M.S. degree in optics from Fudan University, Shanghai, China, in 2013, and the Ph.D. degree in engineering science from Penn State University, University Park, PA, USA, in 2019.

His research focuses on the development and application of acoustophoretic systems and micromotors/swimmers in microfluidics.

**Sudhanshu Tiwari** received the B.Tech. degree in mechanical engineering from A.P.J. Abdul Kalam Technical University, Lucknow, India, in 2015. He is currently pursuing the Ph.D. degree with the Centre for Nano Science and Engineering, Indian Institute of Science, Bengaluru, India.

His research interests include PiezoMEMS design, microfabrication, and vibrational analysis of microelectromechanical system (MEMS) structures.

**Robert R. Benoit** (M'10) received the B.A. degree in physics and math from the Lycoming College, Williamsport, PA, USA, in 2004, and the M.S. and Ph.D. degrees from the University of Virginia (UVA), Charlottesville, VA, USA, in 2007 and 2014, respectively.

He is currently an Electronics Engineer with the Micro and Nano Materials and Devices Branch, U.S. Army Research Laboratory (ARL), Adelphi, MD, USA. At UVA, he studied rapid prototyping of microelectromechanical system (MEMS) devices with focused ion beams and cryogenic radio frequency MEMSs (RF MEMS) for radio astronomy applications. His current research involves piezoelectric RF MEMS with an emphasis on RF switches and packaging techniques.

Dr. Benoit also chairs the Washington DC/Northern VA Chapter, Microwave Theory and Technique Society.

**Yongqiang Qiu** (M'10) received the B.Eng. degree in biomedical engineering from Tianjin University, Tianjin, China, in 2007, and the M.Sc. degree in biomedical engineering and the Ph.D. degree in mechanical engineering from the University of Dundee, Dundee, U.K., in 2009 and 2014, respectively.

He is currently a Lecturer of sensor technologies with the Faculty of Engineering and Technology, Liverpool John Moores University, Liverpool, U.K. His primary research interest is to develop miniature ultrasonic devices and systems for a range of biomedical and industrial applications.

**Holly S. Lay** (M'11) received the B.Sc. degree in electrical engineering and the Ph.D. degree in engineering physics from Queen's University, Kingston, ON, Canada, in 2003 and 2011, respectively.

After working in the industry for two years, she was a Postdoctoral Researcher with the University of Dundee, Dundee, U.K. and the University of Glasgow, Glasgow, U.K, from 2013 to 2018, where she worked on the Sonopill Programme. She is currently an Ultrasound Systems Developer at FUJIFILM VisualSonics, Inc., Toronto, ON, Canada. Her research interests include high-frequency ultrasound, ultrasound electronic systems, and ultrasound device miniaturization.

**Sumit Agrawal** received the B.Tech. degree in electronics and communication from GLA Institute, Mathura, India, in 2012, and the M.Tech. degree in media and sound engineering from IIT Kharagpur, Kharagpur, India, in 2014. He is currently pursuing the Ph.D. degree with Dr. Kothapalli's Group, with a focus on developing dual-modality ultrasound and photoacoustic imaging hardware and image reconstruction software.

He was with KLA, Chennai, India, for one year, where he explored image-processing algorithms for defect inspection in silicon wafers during IC fabrication. He joined SkinCurate Research, Kharagpur, a smart medical imaging devices start-up, where he developed an interest in medical imaging and machine learning.

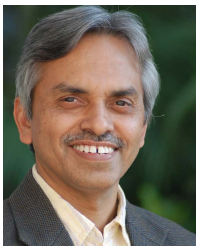

**Rudra Pratap** (SM'02) received the B.Tech. degree (Hons.) from IIT Kharagpur, Kharagpur, India, in 1985, the M.S. degree from The University of Arizona, Tucson, AZ, USA, in 1987, and the Ph.D. degree from Cornell University, Ithaca, NY, USA, in 1993.

He taught at the Sibley School of Mechanical and Aerospace Engineering, Cornell University, from 1994 to 1996. In 1996, he joined the Department of Mechanical Engineering, Indian Institute of Science, Bengaluru, India, as an Assistant Professor, where he served, full time, from 1996 to 2010. He moved to the Centre for Nano Science and Engineering (CeNSE), Bengaluru, as a Professor and the Founding Chairperson. He continues as an Associate Faculty of mechanical engineering. He has been the Deputy Director of the Indian Institute of Science since 2018. His research interests include microelectromechanical system (MEMS) and Nano-Electromechanical Systems, vibroacoustics, bioacoustics, mechano-biology, and computational mechanics.

Dr. Pratap is an elected fellow of the National Academy of Engineering and National Academy of Science. He is also an Associate Editor of the IEEE MICROELECTROMECHANICAL SYSTEMS (MEMS), the *ASME Journal of Microelectromechanical Systems* (MEMS), and the *Journal of Institute of Smart Structures and Systems*.

**Sri-Rajasekhar Kothapalli** received the Ph.D. degree in biomedical engineering from Washington University in St. Louis, St. Louis, MO, USA, in 2009.

He carried out his postdoctoral research at Stanford University, Stanford, CA, USA, from 2009 to 2013. From 2014 to 2016, he was an Instructor with the Department of Radiology, Stanford University. He is currently an Assistant Professor with the Department of Biomedical Engineering, Pennsylvania State University, State College, PA, USA. His research work spans various biomedical imaging techniques, including photoacoustic imaging, ultrasound imaging, and ultrasound-modulated optical tomography (UOT). Working at the interface of microelectromechanical system (MEMS) ultrasound transducer and photoacoustic imaging, he developed CMUT-based dual-modality transrectal ultrasound and photoacoustic (TRUSPA) imaging device for prostate cancer screening and conducted clinical studies on several prostate cancer patients using the TRUSPA device.

**Thomas E. Mallouk** is currently a Vagelos Professor of energy research with the Department of Chemistry, University of Pennsylvania, Philadelphia, PA, USA. His research focuses on the synthesis of inorganic materials and their application to solar energy conversion, catalysis and electrocatalysis, nanoscale and microscale motors, low-dimensional physical phenomena, and environmental remediation. He has authored over 400 publications.

Dr. Mallouk is an Associate Editor of the *Journal of the American Chemical Society*.

**Sandy Cochran** (M'00) received the B.Sc., Ph.D., and M.B.A. degrees from the University of Strathclyde, Glasgow, U.K., in 1986, 1990, and 2001, respectively.

Following work in various research and academic roles from 1990 to 2005 at the University of Strathclyde and the University of the West of Scotland (UWS), Paisley, U.K., he became full-time Professor at UWS in 2005 and moved to the University of Dundee, Dundee, U.K., where he became a Professor in 2010. He is currently a Professor of ultrasound materials and systems with the School of Engineering, University of Glasgow, Glasgow. He has authored over 300 technical publications, proceedings, editorials, and books. His research interests include new piezoelectric materials for ultrasonic transducers, the transducer devices themselves, and their applications in medicine and industry.

Dr. Cochran is currently the Vice President of Ultrasonics of the IEEE Ultrasonics, Ferroelectrics, and Frequency Control Society.

**Susan Trolier-McKinstry** (F'91) is currently a Steward S. Flaschen Professor of ceramic science and engineering, a Professor of electrical engineering, and the Director of the nanofabrication facility, Pennsylvania State University, University Park, PA, USA. Her main research interests include thin films for dielectric and piezoelectric applications. She has authored or coauthored over 400 papers on those topics.

Dr. Trolier-McKinstry has served as the President of the IEEE Ultrasonics, Ferroelectrics, and Frequency Control Society and Keramos. She was the President of the Materials Research Society in 2017. She serves as an Associate Editor for *Applied Physics Letters*.